International Journal of Technology 10(1): 212-221
ISSN 2086-9614

THREE-DIMENSIONAL CFD ANALYSIS OF PERFORMANCE OF SMALL-SCALE HAWT BASED ON MODIFIED NACA-4415 AIRFOIL

Sudarsono[1*], A.A.P Susastriawan[1], Sugianto[2]

[1]*Department of Mechanical Engineering, Institut Sains & Teknologi AKPRIND Yogyakarta, 55222 Indonesia*
[2]*Aeronautical Engineering Program, Department of Mechanical Engineering, State Polytechnic of Bandung, Indonesia*

(Received: July 2018 / Revised: September 2018 / Accepted: January 2019)

ABSTRACT

The geometric of a wind turbine rotor is an important parameter in the development of a horizontal axis wind turbine (HAWT). Simulation can be used to determine the rotor's optimum geometry for specific wind speeds. The present study describes the three-dimensional (3D) computational fluid dynamics (CFD) simulation of a modified small-scale NACA-4415 HAWT rotor in order to predict power output and coefficient, using Blade Element Momentum (BEM) based on Lifting Line Theory (LLT). Power output and coefficient were analysed at wind speeds of 3, 4, 5, 6, and 7 m/s. The results predict that maximum power output increases with increasing wind speed. The predicted minimum power output of 35.41 Watt was obtained at wind speed 3 m/s and Tip Speed Ratio (TSR) 4; the predicted maximum power output was achieved at wind speed 7 m/s and TSR 6. As in the case of power output, power coefficient also improved with rising wind speed, with a coefficient of 0.259 at wind speed 3 m/s and TSR 4 and a coefficient of 0.449 at wind speed 7 m/s and TSR 5. Given Indonesia's typical wind speed of 4 to 5 m/s, this modified NACA-4415 rotor is predicted to generate between 92 and 255 Watts of power. The power output results show good agreement between simulation and experiment, with an R^2 value of 0.93.

Keywords: CFD; HAWT; NACA-4415; Performance; Power

1. INTRODUCTION

As predicted by Sugianto (2016), Indonesia has an approximate wind energy potential of 9.29 GW. Only 500 kW of this potential has been utilized, but it can be optimized by means of a wind turbine energy conversion system. To optimize the design of a wind turbine rotor, it is necessary to consider wind speed characteristics. In Indonesia, wind speed typically ranges from 3 to 7 m/s. An average wind speed of 5 m/s requires a HAWT (Sugianto, 2016). To design a suitable wind turbine for a specific wind velocity, the geometry of the rotor blade (or airfoil) must also be optimal. Figures 1a and 1b illustrate the nature of airfoil aerodynamics in schematic form. Localized pressure (p) and shear force (τ) on the airfoil (Figure 1a) impacts aerodynamic forces that include normal forces (N), lift force (L) and drag force (D) as shown in Figure 1b.

[*]Corresponding author's email: sudarsono1574@akprind.ac.id, Tel. +62-274-563029, Fax. +62-274-563847
Permalink/DOI: https://doi.org/10.14716/ijtech.v10i1.2237

The Reynolds number (Re) for the chord length of the airfoil can be formulated as (Radi et al., 2012; Sugianto, 2016):

$$R_e = \frac{\rho U c}{\mu} \tag{1}$$

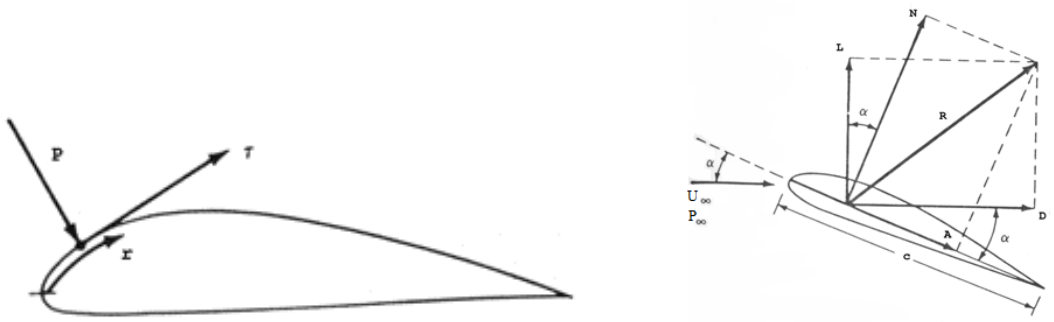

(a) (b)

Figure 1 Schematic diagram of airfoil aerodynamics (Sugianto, 2016)

and the coefficient of pressure (Cp) and coefficient of friction (Cf) can be defined as:

$$C_p = \frac{P - P_\infty}{0.5\rho U_\infty^2} \tag{2}$$

$$C_f = \frac{\tau}{0.5\rho U_\infty^2} \tag{3}$$

Lift force (L), drag force (D), and momentum can be understood as coefficient of lift (Cl), drag Cd), and momentum (Cm) as a function of angle of attack (α) (Radi et al., 2012; Sugianto, 2016):

$$c_l = c_n \cos\alpha - c_a \sin\alpha \tag{4}$$

$$c_d = c_n \sin\alpha + c_a \cos\alpha \tag{5}$$

$$c_{m,1/4chord} = c_m - \frac{1}{4} c_l \tag{6}$$

where C_n is the normal coefficient, and C_a is the axial coefficient. Again following Sugianto (2016) and Radi et al. (2012),

$$c_n = \frac{1}{c}\int_0^c \left(c_{P,lower} - c_{P,upper}\right)dx + \frac{1}{c}\int_0^c \left(c_{f,upper}\frac{dy_{upper}}{dx} + c_{f,lower}\frac{dy_{lower}}{dx}\right)dx \tag{7}$$

$$c_a = \frac{1}{c}\int_0^c \left(c_{P,upper}\frac{dy_{upper}}{dx} - c_{P,lower}\frac{dy_{lower}}{dx}\right)dx + \frac{1}{c}\int_0^c \left(c_{f,upper} + c_{f,lower}\right)dx \tag{8}$$

$$\begin{aligned} c_m = {} & \frac{1}{c^2}\int_0^c \left(c_{P,upper} - c_{P,lower}\right)x dx - \frac{1}{c^2}\int_0^c \left(c_{f,upper}\frac{dy_{upper}}{dx} + c_{f,lower}\frac{dy_{lower}}{dx}\right)x dx + \\ & \frac{1}{c^2}\int_0^c \left(c_{P,upper}\frac{dy_{upper}}{dx} + c_{f,upper}\right)y_{upper}dx + \frac{1}{c^2}\int_0^c \left(c_{f,lower} - c_{P,lower}\frac{dy_{lower}}{dx}\right)y_{lower}dx \end{aligned} \tag{9}$$

The theory of momentum is explained in Figure 2, where air passing through the wind turbine rotor takes the shape of a tube. In Figure 2a, wake is shown by ω and rotational speed of the rotor is indicated by Ω (Ingram, 2011; Sugianto, 2016). Assuming that pressure at point 1 is equal to pressure at point 2 ($p_1 = p_2$), velocity at point 1 is equal to velocity at point 2 ($v_1 = v_2$), with no friction losses from point 1 to point 2 or from point 3 to point 4, the axial induction factor (a) can be defined (Ingram, 2011) as:

$$a = \frac{V_1 - V_2}{V_1} \tag{10}$$

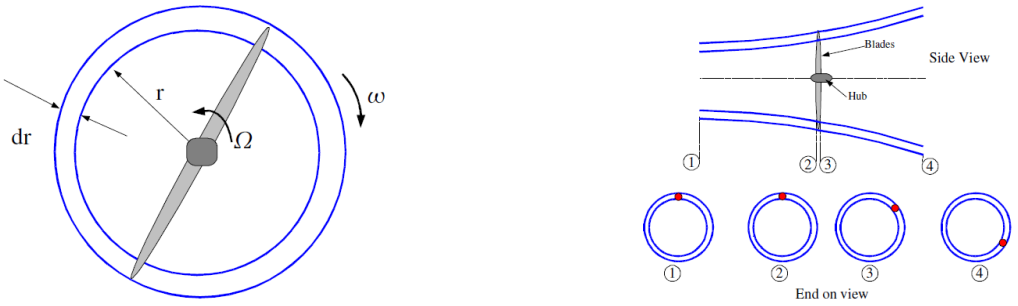

(a) Front view (b) Side view

Figure 2 Cross section of annular tube of the airflow through wind turbine (Ingram, 2011)

Following Sugianto (2016) and Ingram (2011), the angular induction factor can be defined as:

$$a' = \frac{\omega}{2\Omega} \tag{11}$$

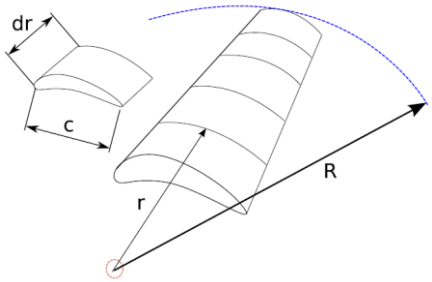

Figure 3 Element model of airfoil (Ingram, 2011)

As Figure 3 indicates, the airfoil comprises several elements, each of which has a different tangential velocity (Ωr), chord, and twist angle. Localized Tip Speed Ratio (TSR) λr is defined by Sugianto (2016) and Ingram (2011) as:

$$\lambda_r = \frac{\Omega r}{U_\infty} \tag{12}$$

and angle of flow β can be formulated as:

$$\tan\beta = \frac{\lambda_r\left(1 + a'\right)}{\left(1 - a\right)} \tag{13}$$

Because of the aerodynamic forces distributed along the airfoil radial, the generated torque is

$$dT = 4a'\left(1 - a\right)\rho U_\infty \Omega \pi r^3 dr \tag{14}$$

and the rotor's total power output is:

$$P = \int_{r_h}^{R} \Omega dT dr \tag{15}$$

Finally, (Ingram, 2011; Sugianto, 2016), the coefficient of power output (Cp) is:

$$C_P = \frac{P}{P_{angin}} = \frac{\int_{r_h}^{R} \Omega dT dr}{\frac{1}{2}\rho\pi R^2 U_\infty^3} = \frac{8}{\lambda^2}\int_{\lambda_h}^{\lambda} \lambda_r^3 a'(1-a)\left[1-\frac{c_d}{c_l}\tan\beta\right] d\lambda_r \tag{16}$$

Equations 1 to 16 can be used for both steady and unsteady state analysis of HAWT and VAWT.

Because wind speed cannot be predicted in a full scale analysis of wind flow, visualization cannot be used; instead, Computational Fluid Dynamics (CFD) was used to analysis wind flow. CFD has previously been used to analysis wind flow by Siswantara et al. (2016) and Daryus et al. (2016). CFD simulation can be used to analysis the Lifting Line Theory (LLT) and the Non Lifting Line Free Vortex Wake Algorithm (LLFVW) as previously reported by Garrel (2003). The LLT have been used to calculate a vortex core model on HAWT as done by Marten et al. (2015), Marten et al. (2016) and Saverin et al. (2016) and by Wendler et al. (2016) for VAWT.

2. METHODS

The CFD analysis involved simulation of the NACA-4415 airfoil and its modification that was followed by simulation of a rotor based the modified airfoil and a modification of HAWT. Figure 4 shows the original NACA-4415 airfoil (red) and its modification (blue).

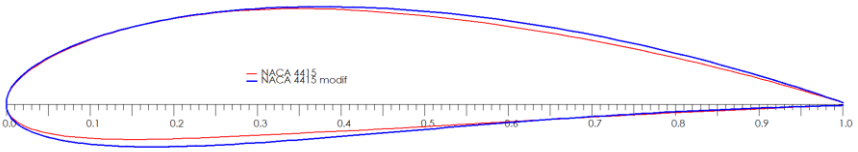

Figure 4 NACA-4415 airfoil and modification

The simulation was performed using a Reynolds number of 4.1×10^4 to 9.6×10^4 for wind speeds of 3 to 7 m/s. In post-processing, coefficients of lift for both airfoils were compared and described as a polar curve to capture aerodynamic performance (Garrel, 2003; Snel et al., 2009). The polar curve for NACA-4415 at wind speed 5 m/s was used to predict rotor performance (Vey et al., 2015; Wendler et al., 2016) at 3 to 7 m/s. Curve fitting for the modified NACA-4415 airfoil followed the Montgomerie method, wherever the HAWT performance is predominantly determined by lift force, curve fitting was based on Cl of the polar curve. To obtain a 360^o polar curve, the blade geometry was based on the 360^o polar curve of the modified NACA-4415 airfoil. The Aerodynamic simulation of the HWAT airfoil blade peformance prioritized to predict coefficient of power (Cp) by analyzing Tip Speed Ratio (TSR). Figure 5 shows the blade geometry based on the modified NACA-4415; the rotor has three blades of diameter 3.25 m.

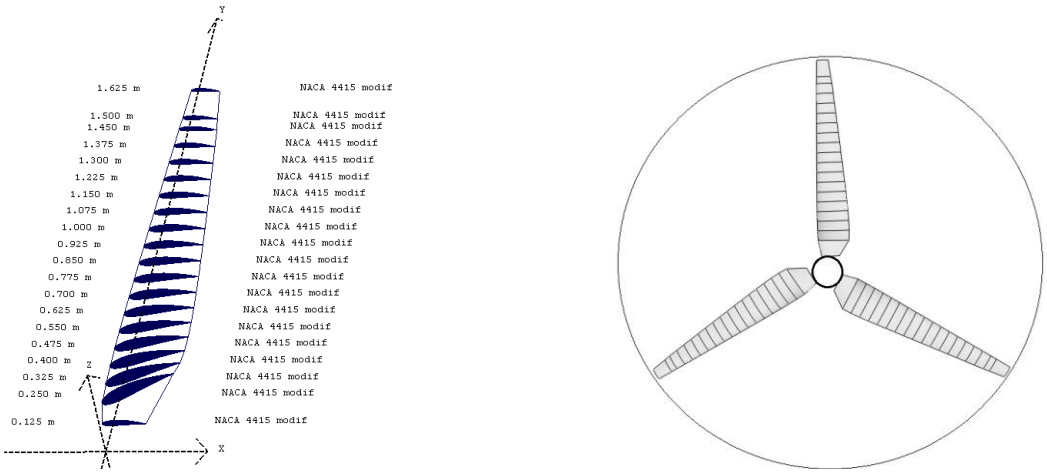

(a) (b)

Figure 5 Geometry of blade based on modified NACA-4415 (a) and (b) the rotor

The HAWT simulation was conducted using Lifting Line Theory (LLT). For the purposes of the CFD simulation, the wind turbine tower was assumed to be 10 m in height. Each wind speed (3, 4, 5, 6 and 7 m/s) was combined with TSR values of 4, 5 and 6, resulting in 15 permutations. The simulation visualized wake wind stream distribution behind the HAWT rotor, and power outputs from the simulations were then compared to experimental data for validation.

3. RESULTS AND DISCUSSION

3.1. Simulation of Airfoil Characteristics

Figure 6 shows the polar curve for lift force coefficients of NACA-4415 and modified NACA-4415 at Reynolds numbers 41000, 55000, 68000, 82000, and 96000 (for wind speeds of 3, 4, 5, 6, and 7 m/s, respectively). From the curve, a dynamic stall area (Bhagwat & Leishman, 2001) can be observed. The curves indicate that the modified NACA-4415 airfoil produces a higher C_l at the same angle; using the Montgomerie method to obtain a 360^o polar curve, the result of curve fitting is shown in Figure 7.

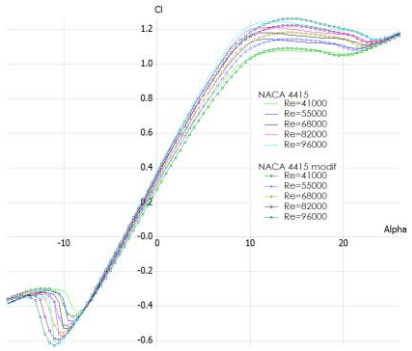

Figure 6 Polar curve of Cl on alpha at Re = 4.1×10^4 to 96×10^4

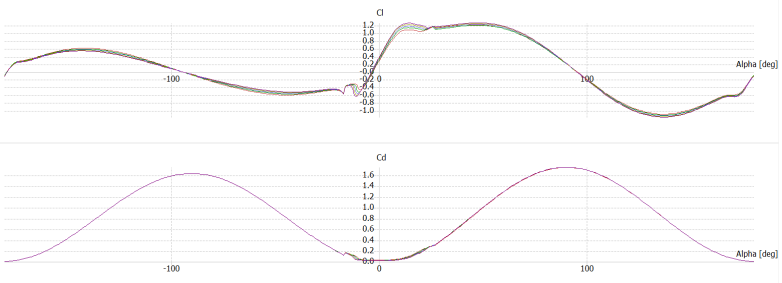

Figure 7 360^o polar curve Cl on alpha at Re = 4.1×10^4 to 9.6×10^4

3.2. Simulation of the Rotor

Figure 8 shows the results of the rotor simulation. For all Reynold numbers, C_p increases for 0 < TSR < 5 and decreases for 5 < TSR < 10. The graph indicates that a TSR of 5 produces the highest C_p.

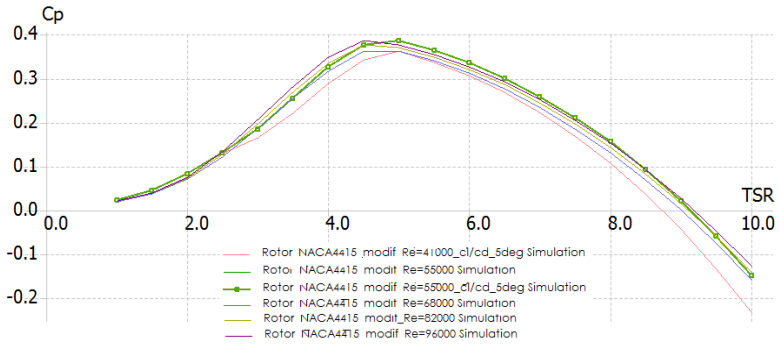

Figure 8 Cp×TSR

3.3. Simulation of Wind Stream using Lifting Line Theory

The results of CFD simulation of wake wind stream after passing through the rotor for wind speeds of 3, 4, 5, 6, and 7 m/s combined with varying TSR values of 4, 5, and 6 are shown in Figures 9, 10, 11, 12, and 13.

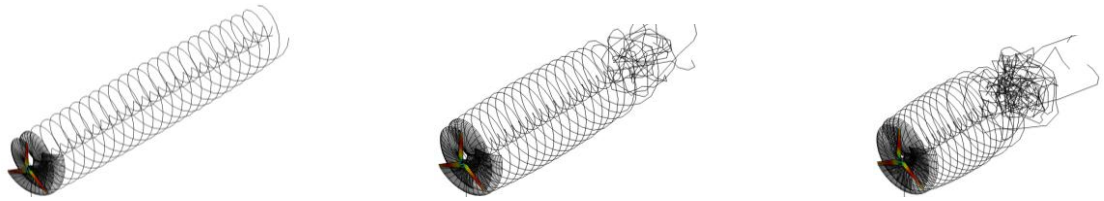

(a) (b) (c)

Figure 9 Wake wind stream after passing through the turbine rotor at a wind speed of 3 m/s with TSR: (a) 4; (b) 5; and (c) 6

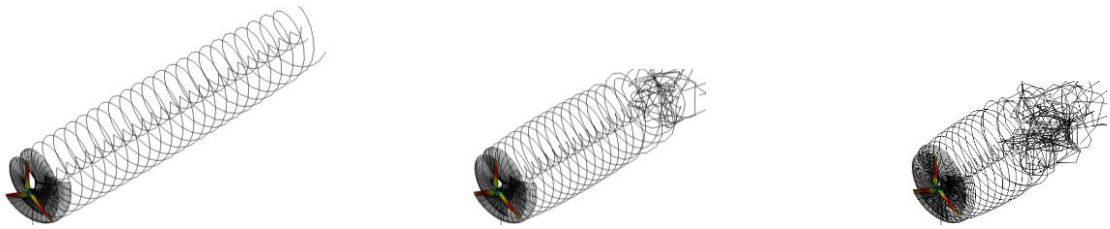

(a) (b) (c)

Figure 10 Wake wind stream after passing through the turbine rotor at a wind speed of 4 m/s with TSR: (a) 4; (b) 5; and (c) 6

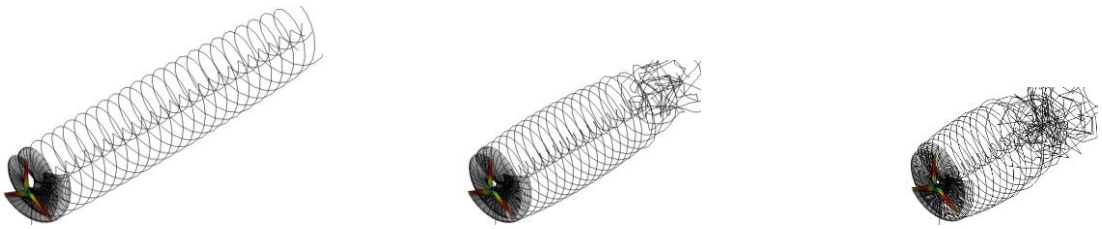

(a) (b) (c)

Figure 11 Wake wind stream after passing through the turbine rotor at a wind speed of 5 m/s with TSR: (a) 4; (b) 5; and (c) 6

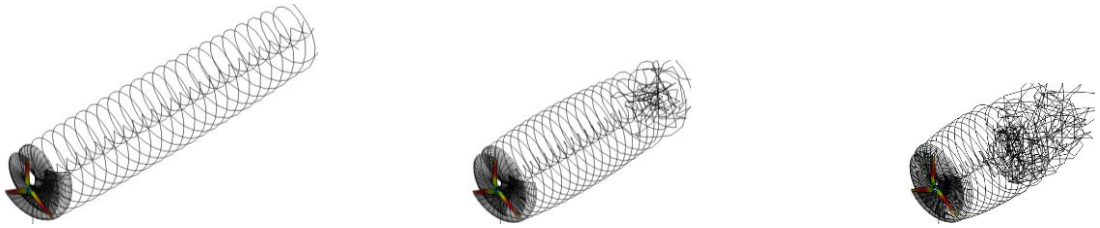

(a) (b) (c)

Figure 12 Wake wind stream after passing through the turbine rotor at a wind speed of 6 m/s with TSR: (a) 4; (b) 5; and (c) 6

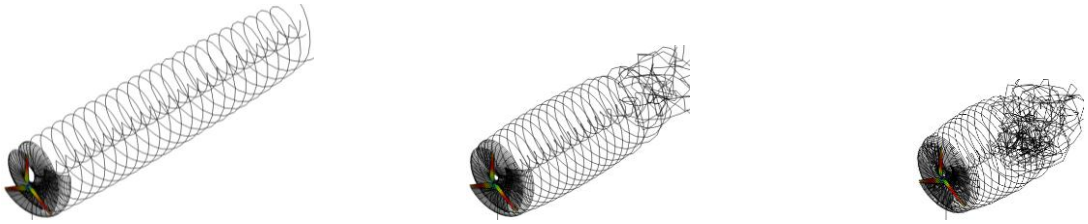

(a) (b) (c)

Figure 13 Wake wind stream after passing through the turbine rotor at a wind speed of 7 m/s with TSR: (a) 4; (b) 5; and (c) 6

The wake wind streams in Figures 9 to Figure 13 indicate that TSR increases from 4 to 6, causing wake length to decrease. The decrease in wind stream wavelength was affected by increased speed of rotor rotation. The effect of changes in TSR on wake wavelength was highly significant. This differed from wind speed; increasing wind speed did not affect wake wind stream, and wind speed does not cause a change in wavelength at a constant TSR.

Figures 14 to 16 compare wake formation for the original and modified blades at a wind speed of 3 m/s for TSR 4, 5, and 6. For each TSR, wake length behind the original blade is relatively shorter than for the modified blades, indicating that the modified blade generates more power than the original.

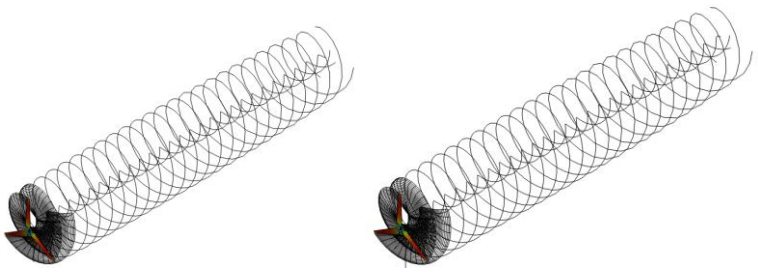

Figure 14 Wake wind stream after passing through the turbine rotor (left: original and right: modified) at a wind speed of 3 m/s with TSR 4

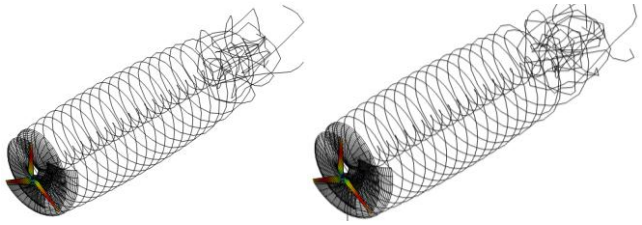

Figure 15 Wake wind stream after passing through the turbine rotor (left: original and right: modified) at a wind speed of 3 m/s with TSR 5

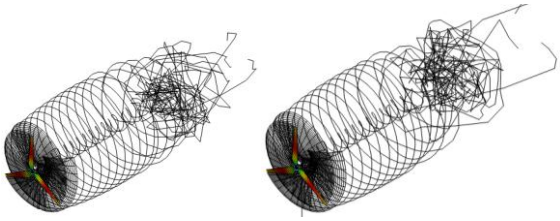

Figure 16 Wake wind stream after passing through the turbine rotor (left: original and right: modified) at a wind speed of 3 m/s with TSR 6

3.4. Simulation of HAWT

Wake velocity distribution behind the rotor can be understood in terms of various components of velocity. Figures 17 and 18 show X, Y, and Z components of velocity for wind speed 3 m/s at TSR 4 and 5, respectively. At a wind speed of 3 m/s, wake velocities for X, Y, and Z increase as TSR increases from 4 to 5. Aerodynamically, the wake pattern behind the rotor affects turbine power output.

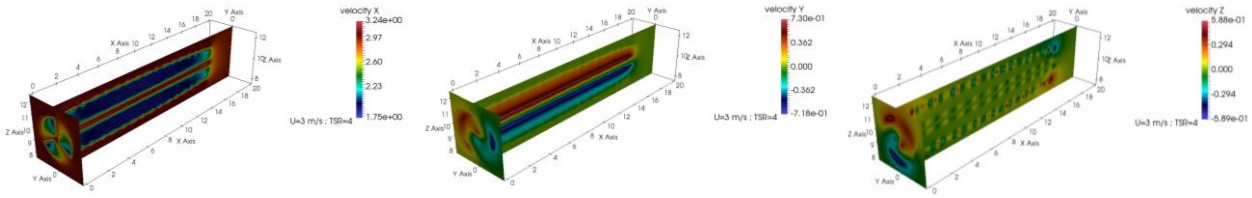

X-component velocity Y-component velocity Z-component velocity

Figure 17 Wake velocity distribution at wind speed 3 m/s and TSR 4

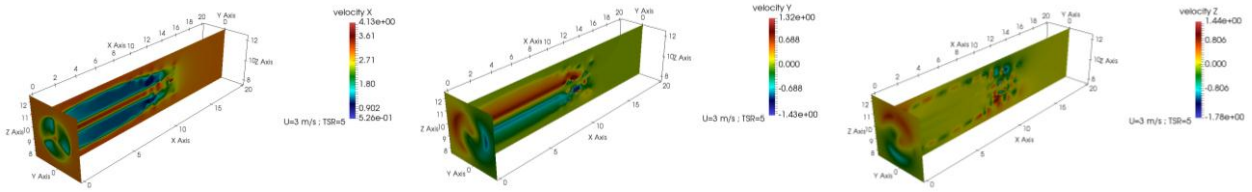

X-component velocity Y-component velocity Z-component velocity

Figure 18 Wake velocity distribution at wind speed 3 m/s and TSR 5

Table 1 Predicted power and coefficient of power

U (m/s)	TSR	N (rpm)	Power		Cp	
			Original (Watt)	Modified (Watt)	Original	Modified
3	4	70.74	34.62	35.41	0.253	0.259
3	5	88.42	49.70	49.73	0.364	0.365
3	6	106.11	50.30	49.49	0.369	0.363
4	4	94.31	90.59	92.25	0.280	0.285
4	5	117.89	130.35	128.88	0.403	0.399
4	6	141.47	126.35	123.82	0.390	0.383
5	4	117.89	189.04	193.25	0.299	0.306
5	5	147.37	268.51	265.64	0.425	0.421
5	6	176.84	255.68	255.17	0.405	0.404
6	4	141.47	346.36	355.75	0.317	0.326
6	5	176.84	482.79	477.05	0.442	0.437
6	6	212.21	462.11	446.02	0.423	0.409
7	4	165.05	579.21	595.01	0.334	0.344
7	5	206.31	787.49	778.97	0.454	0.449
7	6	247.57	718.55	726.61	0.414	0.419

Integrating equations 15 and 16 to obtain power output and coefficient of power, the results in Table 1 show that the modified blade produces a higher c_p and power output at TSR 4 for all of the simulated wind speeds.

For the purpose of validation, power outputs obtained from the simulation were compared to experimental data. As shown in Figure 19 (simulation and experimental results in red and blue, respectively), the high correlation between simulation and experimental data for power output confirms that the simulation was valid, with an R^2 value of 0.93.

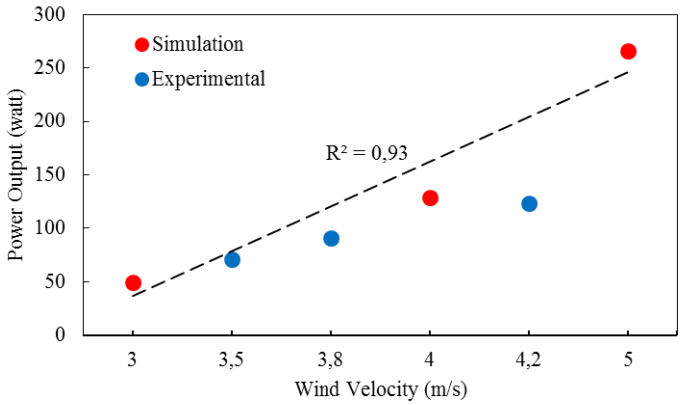

Figure 19 Validation of simulation by comparison with experimental data

4. CONCLUSION

It can be concluded that the simulation was effective in predicting the power output of a small-scale HAWT based on a modified NACA-4415 airfoil. The rotor is predicted to generate power in the range of 92–255 Watts at a typical Indonesian wind speed of 4 to 5 m/s, with a high correlation between simulation and experimental data ($R^2 = 0.93$).

5. ACKNOWLEDGEMENT

This study was funded by Ministry of Research, Technology and Higher Education of the Republic of Indonesia, Directorate General of Strengthening Research and Development, and LLDIKTI V Yogyakarta with contract number: 061/HB-LIT/IV/2017, 14 April 2017. The author wish to thank Institut Sains & Teknologi AKPRIND Yogyakarta for the support.

6. REFERENCES

Bhagwat, M.J., Leishman G.J., 2001. Stability, Consistency and Convergence of Time-marching Free-vortex Rotor Wake Algorithms. *Journal of the American Helicopter Society*, Volume 46(1), pp. 46–59

Daryus, A., Siswantara, A.I., Darmawan, S., Gunadi, G.G.R., Camalia, R., 2016. CFD Simulation of Turbulent Flows in Proto X-3 Bioenergy Micro Gas Turbine Combustor using STD *k-ε* and RNG *k-ε* Model for Green Building Application. *International Journal of Technology*, Volume 7(2), pp. 204–211

Garrel, A.V., 2003. *Development of a Wind Turbine Aerodynamics Simulation Module*. Netherlands: ECN

Ingram, G., 2011. Wind Turbine Blade Analysis using the Blade Element Momentum Method. Durham University. Available Online at https://community.dur.ac.uk/g.l.ingram/download/wind_turbine_design.pdf

Marten, D., Lennie, M., Pechlivanoglou, G., Nayeri, C.N., Paschereit, C.O., 2015. Implementation Optimization and Validation of a Nonlinear Lifting Line Free Vortex Wake Module within the Wind Turbine Simulation Code QBlade. *Journal of Engineering for Gas Turbines and Power*, Volume 138(7), pp. 1–11

Marten, D., Pechlivanoglou, G., Nayeri, C.N, Paschereit, C.O., 2016. Nonlinear Lifting Line Theory Applied to Vertical Axis Wind Turbines: Development of a Practical Design Tool. *In*: 16th International Symposium on Transport Phenomena and Dynamics of Rotating Machinery April 10-15, Honolulu, USA ISROMAC

Radi, S.K., Tria, M.A., Sugianto, 2012. Simulasi Numerik Pengaruh Protuberance pada Koefisien Aerodinamika Airfoil NACA 631412 pada Kecepatan Subsonik *(Numerical Simulation Effect of Protuberance on the Aerodynamic Coefficient of Airfoil NACA 631412 at Subsonic Speed). Journal of MeTrik Polban*, Volume 6(2), pp. 26–44

Saverin, J., Marten, D., Pechlivanoglou, G., Nayeri, C.N., Paschereit, C.O., 2016. Coupling of an Unsteady Lifting Line Free Vortex Wake Code to the Aeroelastic HAWT Simulation Suite FAST. *In*: ASME paper GT2016-56290, ASME Turbo Expo 2016, June 13–17, Seoul, South Korea

Siswantara, A.I., Daryus, A., Darmawan, S., Gunadi, G.G.R., Camalia, R., 2016. CFD Analysis of Slurry Flow in an Anaerobic Digester. *International Journal of Technology*, Volume 7(2), pp. 197–203

Snel, H., Schepers, J.G., Siccama, N., 2009. Mexico Project: The Database and Results of Data Processing and Interpretation. *In*: 47th AIAA Aerospace Sciences Meeting, USA

Sugianto, 2016. Simulasi Numerik Pengembangan TASH Berbasis Sudu Sandia-Seri 8 Setara M20 Kw *(Numerical Simulation for Development of the Horizontal Wind Axis Turbine (HAWT) Base on Sandia-8 Series Equivalent M20-Kw). In*: Proceedings of Mechanical and Vocational Technology National Conference, pp. 204–214

Vey, S., Marten, D., Pechlivanoglou, G., Nayeri, C.N., C.O, 2015. Paschereit, Experimental and Numerical Investigations of a Small Research Wind Turbine. *In*: 33rd AIAAA Applied Aerodynamics Conference, Dallas, Texas

Wendler, J., Marten, D., Pechlivanoglou, G., Nayeri, C.N., Paschereit, C.O., 2016. Implementation and Validation of an Unsteady Aerodynamics Model for Horizontal and Vertical Axis Wind Turbine within the Simulation Tool. *In*: ASME paper GT2016-57184, ASME Turbo Expo 2016, June 13–17, Seoul, South Korea